HHS Public Access

Author manuscript

ACS Appl Mater Interfaces. Author manuscript; available in PMC 2017 November 30.

Published in final edited form as:

ACS Appl Mater Interfaces. 2016 November 30; 8(47): 32450–32459. doi:10.1021/acsami.6b10538.

Hypoxia-Mimicking Nanofibrous Scaffolds Promote Endogenous Bone Regeneration

Qingqing Yao[†,‡], **Yangxi Liu**[†,‡], **Jianning Tao**[§], **Keith M. Baumgarten**[||], and **Hongli Sun**[†,‡,*]

[†]Department of Biomedical Engineering, University of South Dakota, Sioux Falls, South Dakota 57107, United States

[‡]BioSNTR, Sioux Falls, South Dakota 57107, United States

[§]Children's Health Research Center at Sanford Research, Sioux Falls, South Dakota 57104, United States

[||]Orthopedic Institute, Sioux Falls, South Dakota 57105, United States

Abstract

Utilizing biomimetic materials to potentiate endogenous cell growth or signaling is superior to relying on exogenous cells or signals for bone formation. Desferoxamine (DFO), which is a hypoxia-mimetic agent that chelates iron (Fe^{3+}), mimics hypoxia to encourage bone healing. However, high cytotoxicity, off-target effects, and the short half-life of DFO have significantly impeded its further applications. We mitigated these side effects by locally immobilizing DFO onto a gelatin nanofibrous (GF) scaffold that retained DFO's ability to chelate Fe^{3+}. Moreover, DFO-functionalized GF (GF-DFO) scaffolds, which have similar micro/macrostructures to GF scaffolds, not only demonstrated decreased cytotoxicity on both human umbilical vein endothelial cells and human mesenchymal stem cells but also significantly increased vascular endothelial growth factor (VEGF) expression in vitro. Most importantly, in our in vivo experiments on a critical-sized cranial bone defect mouse model, a significant amount of bone was formed in most of the GF-DFO scaffolds after six weeks, while very little new bone was observed in the GF scaffolds. These data suggest that use of a hypoxia-mimicking nanofibrous scaffold is a promising strategy for promoting endogenous bone formation.

Graphical Abstract

[*]Corresponding Author: Phone: (+1) 605-275-7470; Fax: +1 605-782-3280; Hongli.Sun@usd.edu.

ORCID

Jianning Tao: 0000-0001-5678-9272

The authors declare no competing financial interest.

Supporting Information

The Supporting Information is available free of charge on the ACS Publications website at DOI: 10.1021/acsami.6b10538.

High magnification SEM images of gelatin nanofibers (PDF)

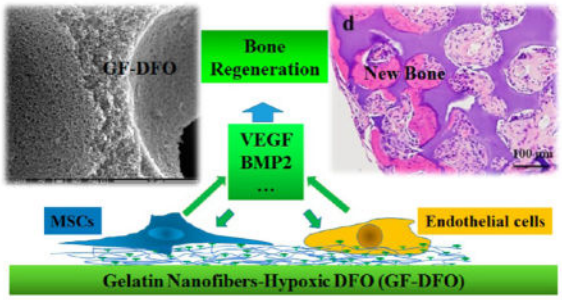

Keywords

hypoxia; desferoxamine; nanofibrous scaffold; angiogenesis; endogenous bone regeneration

1. INTRODUCTION

Repair of large bone defects caused by tumor resection, trauma, infection, and congenital malformation remains a significant, unmet clinical challenge. Biomaterial-mediated exogenous stem/progenitor cell (e.g., bone marrow mesenchymal stem cells, BMSCs) transplantation and growth factor/hormone (e.g., bone morphogenetic proteins, BMPs) delivery are two widely studied alternative approaches for large bone defect repair. Safety and cost concerns have limited the therapeutic translation of these approaches.[1–4]

New biomaterials that mimic physiological osteogenic processes by potentiating endogenous reparative cells/signals will mitigate the safety and cost concerns associated with exogenous cells/growth factors. Osteogenesis is tightly coupled with angiogenesis through hypoxia-inducible factor-1 alpha (HIF-1α).[5,6] Hence, fast vascularization is critical for successful bone regeneration, especially for critical-sized bone defects.[7,8] Because angiogenesis is a complex, cocoordinated process that involves multiple-factors,[9,10] promoting vascularization in engineered tissues by delivering just one or two growth factors (e.g., vascular endothelial growth factor, VEGF, and fibroblast growth factor, FGF) remains a challenge. As the key upstream transcription factor response to hypoxia stress, HIF-1α plays critical roles in tissue regeneration, including regeneration of bone tissue[5,6,11,12] through generation of VEGF,[12,13] stromal cell-derived factor 1 (SDF-1), and other reparative signals for angiogenesis and progenitor cells recruitment.[14,15] Therefore, we speculated that a hypoxia-mimetic agent-immobilized scaffold could strongly activate HIF-1α-mediated angiogenesis, thus promoting bone healing.

Desferoxamine (DFO) is an FDA-approved iron chelator for iron overload diseases.[16–18] DFO is a potent hypoxia-mimetic agent because its iron chelating ability vigorously inhibits the activity of prolyl hydroxylase enzyme (PHD), which is the key enzyme responsible for the degradation of HIF-1α.[19] Thus, DFO can activate HIF-1α and subsequently angiogenesis.[19,20] Whether locally or systemically injected, DFO has shown promise in promoting bone regeneration.[5,12,19,21,22] However, its further application is significantly impeded by a short plasma half-life (~5.5 min) and high drug toxicity.[23,24] High dosage of DFO, normally required due to its low efficacy, can cause severe growth retardation,

endocrine dysfunction, and peripheral neuropathies.[25] It has been reported that covalent attachment of DFO onto biocompatible polymers (e.g., dextran, starch, poly(ethylene glycol) [PEG], and polyglycerol) is a valid method of reducing its toxicity and extending its half-life while simultaneously retaining its chelating ability.[24–26] These blood compatible and degradable DFO-polymer macromolecules are thought to be promising for long circulating, nontoxic iron chelators.[26] However, these freely mobile DFO-polymer macromolecules still have the potential to produce off-target effects after injection into the body even though the direct cytotoxicity is low. Therefore, we expect that localized delivery of covalently bounded DFO on a solid polymeric scaffold/substrate will address this challenge and be appealing for tissue engineering application.

Gelatin, the partially denatured derivative of collagen, is chemically similar to collagen, which is the most abundant protein in bone organic matrix (>90%). Combining the thermally induced phase separation (TIPS) method with the particle leach technique (TIPS&P), gelatin nanofibrous (GF) scaffolds can be fabricated. These scaffolds facilitate osteogenic differentiation and bone formation because they mimic both the physical structure and the chemical composition of the native bone matrix.[27–29] Furthermore, GF scaffold is an ideal platform for DFO immobilization due to the abundant carboxyl groups on gelatin that are available for cross-linking to the amino groups of DFO and the high surface area of the nanofibrous structure, which is suitable for a high amount of drug immobilization.

In the present work, our central hypothesis is that the covalent conjugation of DFO with a polymeric scaffold can decrease its toxicity, elongate its half-life, and promote bone tissue regeneration through locally activating endogenous hypoxia mediated-angiogenesis and potentially other reparative cells and signals.

2. MATERIALS AND METHODS

2.1. Materials

Gelatin type B (from bovine skin, 225 Bloom), (2-(*N*-morpholino) ethanesulfonic acid) hydrate (MES), *N*-hydroxy-succinimide (NHS), and cyclohexane were purchased from Sigma (St. Louis MO, United States). Deferoxamine mesylate was purchased from Abcam (Abcam, Cambridge, MA, United States). Ethanol, 1, 4-dioxane, and hexane were purchased from Fisher Scientific (New Jersey, United States). 1-Ethyl-3-(3-(dimethylamino)propyl) carbodiimide HCl (EDC) was purchased from Thermal Scientific (Rockford, United States).

2.2. Preparation of 2D and 3D NF Gelatin Scaffolds

Both 2D and 3D NF gelatin scaffolds were prepared as previously described.[30] Paraffin spheres with a diameter size between 150 and 300 μm were prepared and used for 3D NF gelatin scaffold preparation. The gelatin-paraffin scaffolds were cut into ϕ 5 × 1 mm discs and then immersed into hexane to remove paraffin spheres. After that, cyclohexane was used to exchange the hexane. The samples were freeze-dried in a salt-ice bath for 48 h and stored in a desiccator. The chemical cross-linking of 2D and 3D GF scaffolds was carried out in the MES buffer (pH 5.3, 0.05 M) with EDC and NHS as cross-linker on ice for 24 h. For the GF-DFO samples, DFO with different concentrations was added into EDC/NHS solution.

After cross-linking, the GF and GF-DFO scaffolds were washed with distilled (DI) water 3 times and then frozen at −20 °C overnight and freeze-dried for 48 h.

2.3. Physical-Chemical Characterization of 2D and 3D GF Scaffolds

The morphology and microstructure of 2D and 3D GF scaffolds were studied using Quanta standard Environmental SEM (FEI, United States).

The porosity (p) of the GF scaffold was calculated by measurement of their mass and dimensions and applying the equation

$$P_{\text{scaffold}} = [1 - \rho_{\text{a}}/\rho_{\text{s}}] \times 100\% \quad (1)$$

where ρ_{a} is the apparent density of the gelatin scaffolds computed by measuring their mass (m) and volume (V) (i.e., $\rho_{\text{a}} = m/V$). The density of gelatin B is 1.35 g/cm^3.

Iron chelation measurement was detected using gelatin-DFO. Briefly, 10 mg of gelatin B was dissolved in 5 mL of MES buffer (pH 5.3) contained in EDC/NHS at 40 °C for 1 h, and the solution was cooled to room temperature. Ten milligrams of DFO was added to the solution, and it was incubated for 24 h at room temperature. The mixture solution was then transferred to a dialysis cassette (MWCO 2000, Thermal Scientifc) and dialyzed for 3 days (fresh DI water was replaced every 12 h). After that, the solution was frozen at −20 °C overnight and freeze-dried for 24 h. The prepared gelatin-DFO powder was dissolved in a 3 mM ferric chloride ($FeCl_3$, Sigma) solution and measured the absorption peak using a UV–vis spectroscopy (DU 730, Beckman coulter).

To study the in vitro release of DFO from GF scaffolds, 1 mL of 10 mM DFO was either cross-linked to GF scaffolds by EDC/NHS as described above or the same amount of DFO was physically absorbed to the GF scaffolds as the control group. Each prepared scaffold was then immersed in 1 mL of a pure water solution at 37 °C on an orbital shaker at a speed of 90 rpm for 10 days. Half of the solution in each vial was collected and refilled at each time point. The amount of DFO release was measured by integrating with a certain amount of $FeCl_3$ and determined using a UV spectrophotometer at 485 nm, as previously described.[31] After 10 days of release, the retained DFO in the GF scaffold was visualized by incubating in 6 mM $FeCl_3$ solution for 10 min at room temperature. GF scaffolds without DFO were included as the negative control group.

2.4. In Vitro Cell Studies

2.4.1. Cell Viability and Morphology Studies—Both hMSCs and HUVECs were obtained from Lonza (Walkersville, MD, United States). The cytotoxicity of DFO and GF-DFO scaffolds on HUVECs and hMSCs was studied using MTS assay (Promega Corporation, United States) according to the manufacturer's instructions. For the study of cytotoxicity of DFO, HUVECs and hMSCs (5×10^3 cells per well) were cultured in a 96-well plate at 37°C and 5% CO_2 for 1, 3, and 5 days. The cell viability was expressed as 100% for the cells cultured in growth medium. For the study of cytotoxicity of GF-DFO,

HUVECs and hMSCs (5×10^4 cells per well) were seeded onto GF or GF-DFO scaffolds and cultured for 1 and 5 days. GF scaffolds without DFO were involved as controls, and the cell viability was expressed as 100%. The morphologies of HUVECs and hMSCs on the GF and GF-DFO scaffolds were visualized by staining with Texas Red-X Phalloidin (Molecular Probes, Grand Island, NY) and DAPI (SouthernBiotech, Birminghan, AL) according to the manufacturer's manual. The stained cells were observed under confocal microscopy (FV1200, Olympus, Japan).

2.4.2. Enzyme Linked Immunosorbent Assay (ELISA)—HUVECs and hMSCs (5×10^4 cells per well) were seeded into a 24-well plate and incubated overnight at 37 °C and 5% CO_2. The culture medium was supplemented with different concentrations of DFO and cultured for another 24 or 48 h. After that, the amount of VEGF and bone morphogenetic protein 2 (BMP2) in the supernatant were measured using human VEGF and human BMP2 ELISA development kit (Peprotech, Rocky Hill, NJ, United States), respectively, according to the manufacturers' protocols. A microplate reader (Infinite M200, Tecan) was used to measure the medium's absorbance at 405 nm with wavelength correction set at 650 nm. For the study of VEGF expression on scaffolds, HUVECs (3×10^5 cells per scaffold) and hMSCs (1×10^5 cells per scaffold) were seeded onto GF and GF-DFO scaffolds and cultured for 24 h. GF scaffolds without DFO were used as controls.

2.5. Bone Regeneration in Vivo

2.5.1. Critical-Sized Cranial Bone Defect Model—Care and use of the laboratory animals followed the protocol approved by the Institutional Animal Care and Use Committee (IACUC) of the University of South Dakota. Inbred C57BL/6NHsd male mice (5–6 weeks, Envigo) were used to create critical-sized cranial bone defect model for in vivo study, as we previously described.[32] Sterile GF and GF-DFO scaffolds (Φ 5 × 1 mm) were directly placed in the cranial defects, and the overlying tissue was closed with surgical staples. Recombinant human BMP2 (1.5 μg, rhBMP2, Peprotech, Rocky Hill, NJ, United States) was resuspended in 10 μL of collagen I (Bedford, MA, United States) and then incorporated into GF scaffolds. These collagen/BMP2 GF scaffolds served as a positive control (BMP2 group), while cranial defects without scaffolds implanted were used as the blank control (blank group). All mice were euthanized six weeks after surgery. Retrieved samples were fixed in 10% formalin for couple of days and then moved into 70% ethanol for further analysis.

2.5.2. Radiographic and Histological Analysis—Radiographic analysis was performed on the fixed constructs using an In-Vivo Xtreme small animal imaging system (Bruker, Billerica, MA, United States). The formalin fixed samples were decalcified with 15% EDTA (pH 7.2) solution for 3 days before they were embedded in paraffin for further histological analysis. Cross sections (5 μm) were cut from the middle of scaffolds and stained with hematoxylin and eosin (H&E) for microscopic observation. The percentage of new bone area of each specimen (new bone area in scaffold/total scaffold area × 100%) was measured using the ImageJ software.

2.6. Statistical Analysis and Image Editing

To determine statistical significance of observed differences between the study groups, a two-tailed homoscedastic *t*-test was applied. A value of $p < 0.05$ was considered to be statistically significant. Values are reported as the mean ± standard deviation (SD). Brightness and contrast were adjusted equally across all images for improved visibility.

3. RESULTS

3.1. Cytotoxicity of DFO on HUVECs and hMSCs

Native DFO showed significant cytotoxicity on both HUVECs and hMSCs from the MTS assay (Figure 1). The considerable cytotoxicity of DFO on HUVECs was noticeable as early as 1 day after culture (Figure 1A). Moreover, cell viability continually decreased as the incubation time increased. On the fifth day, the lowest cell viability was around 25% in contrast to the cell viability of the control group. Compared to HUVECs, hMSCs seemed more resistant to DFO treatment (Figure 1B). There was no noticeable cytotoxicity after 1 day of cell culture of hMSCs at all the tested concentrations of DFO. However, after three days, significant cytotoxicity was observed. Consistent with the observations in HUVECs, cytotoxicity elevated as the culture time increased.

3.2. VEGF and BMP2 Expression Induced by DFO in HUVECs and hMSCs

The expressions of VEGF and BMP2 responses to DFO treatment were very different in HUVECs and hMSCs (Figure 2). Only the 250 μM concentration of DFO significantly increased VEGF expression in HUVECs after 24 h of culture. Even at elevated concentration of DFO, the highest VEGF concentration level (less than 2 pg/μg total protein) in HUVECs was still considered very low (Figure 2A). Compared to the mild responses of HUVECs, the hMSCs indicated a much higher level of VEGF expression response to DFO treatment (Figure 2B). Moreover, DFO significantly increased VEGF expression at a low concentration (20 μM) and further increased VEGF level in a dose dependent manner. When the expression of BMP2 without DFO is examined, HUVECs had an expression level much higher than that of hMSCs, and when DFO was added, it significantly increased BMP2 expression in HUVECs further than in hMSCs after 24 and 48 h of treatment.

3.3. Scaffold Characterization

On the basis of our measurements, the gelatin scaffolds had macro- and microstructures very similar to those of the previous reports.[30] Detailed structural parameters are listed in Table 1. Slightly different microstructures between 3D and 2D GF scaffolds were observed. The nanofiber diameter (130 ± 42 nm) of the 3D GF scaffolds was smaller compared with the nanofiber diameter (180 ± 54 nm) of the 2D GF scaffolds. Furthermore, the nanofiber length (716 ± 175 nm) of the 3D GF scaffolds was shorter compared with the nanofiber length (1070 ± 232 nm) of the 2D GF scaffolds. Finally, the porosity (95.90 ± 0.64%) of 3D GF scaffolds was slightly higher than 2D GF scaffolds (89.17 ± 0.13%), although both can be considered highly porous. Interconnected macropore structures, which are essential for cells and tissue ingrowth, were created using assembled paraffin spheres (150–300 μm). It was

noted that covalently cross-linked DFO on gelatin did not change the nanofibrous structure of 2D or 3D GF scaffolds (Figure 3 and Figure S1).

3.4. Iron Binding Ability of GF-DFO and in Vitro DFO Release

Both DFO-Fe^{3+} (as a positive control) and gelatin-DFO-Fe^{3+} (Figure 4A) had a broad absorption peak at around 429 nm, which is the characteristic absorption peak of DFO-Fe^{3+}.[26] Without Fe^{3+}, DFO and gelatin-DFO-only samples (as negative controls) showed no absorption peak at 429 nm. The iron binding property of gelatin-DFO indicated that DFO retained its chelating ability to Fe^{3+} after covalent conjugation with gelatin. These data were critical for the following studies because the iron chelating ability is the main mechanism for DFO's hypoxia-mimetic function.[19]

To study the in vitro release of DFO from GF scaffolds, the same amounts of DFO were either physically absorbed or chemically cross-linked onto GF scaffolds. As the data show (Figure 4B), both groups had a typical burst release in the first few days, which suggested that an overdose of DFO was added for cross-linking, and most of the released DFO was from physical absorption. However, it was noted that significantly more DFO was released from the cross-linked group on days 7 and 10 compared to that released from the physically absorbed group. Moreover, after 10 days of release, a significantly higher amount of functional DFO was retained in the cross-linked scaffolds compared to that retained in the absorbed scaffolds according to the color derived from the captured Fe^{3+} (the inset of Figure 4 B).

3.5. Cell Viability and Morphology on GF-DFO Scaffolds

Initial DFO concentrations for cross-linking onto GF scaffolds were 100 μM (GF-DFO 100 μM) and 1 mM (GF-DFO 1 mM). GF-DFO scaffolds exhibited no detrimental effects on HUVECs on both 1 and 5 days of cell culture (Figures 5A1 and A2). However, significant cytotoxicity was noticed when the initial DFO concentration was increased to 10 mM (GF-DFO 10 mM) after 1 and 5 days of culture. Ten millimolar was the highest DFO concentration that can be dissolved in the cross-linking solution in our studies. The cell viability of HUVECs on GF-DFO 10 mM scaffolds was around 70% compared with that of the control group (GF scaffolds only) at both day 1 and 5. We observed very different responses of HUVECs on GF-DFO compared to the free DFO. No dose or time dependent cytotoxicity was observed on GF-DFO scaffolds (Figures 5A1 and A2), which was different from what was found in the free DFO solutions (Figure 1). Moreover, no cytotoxicity was observed on GF-DFO 10 mM scaffolds for hMSCs (Figure 5A2) as well. This result was consistent with the data from the free DFO studies for hMSCs (Figure 1) and suggested that hMSCs were more resistant to DFO stress. Additionally, cell morphology of HUVECs and hMSCs on DFO-decorated GF scaffolds were investigated (Figure 5B). Confocal imaging demonstrated HUVECs and hMSCs were able to attach and spread on both GF and GF-DFO scaffolds after 16 h of culture. No obvious differences in cell morphology of HUVECs and hMSCs were observed between the GF and GF-DFO scaffolds.

3.6. VEGF Expression of HUVECs and hMSCs on GF-DFO Scaffolds

From the ELISA results, DFO modified GF scaffolds (GF-DFO) significantly increased VEGF expression in both HUVECs and hMSCs after 24 h (Figure 6). VEGF expression in HUVECs increased more than twofold on GF-DFO 10 mM scaffolds. When the VEGF expression change in HUVECs response is compared to that in free DFO, the functional DFO in the GF-DFO 10 mM scaffolds should be more than 250 μM because the free DFO at 250 μM increased VEGF expression less than twofold in HUVECs (Figure 2). Furthermore, the cytotoxicity of GF-DFO 10 mM scaffolds was much lower than that in free 250 μM DFO at day 5 (70 vs 25% cell viability, see Figures 1 and 5A1). Similarly, GF-DFO scaffolds also significantly elevated VEGF expression in hMSCs, although the change was not as high as the response to free DFO (right panel, Figure 6). These data suggested that covalent immobilization of DFO onto GF scaffolds can significantly reduce DFO's cytotoxicity while retaining its activity.

3.7. GF-DFO Scaffolds Promote Endogenous Bone Regeneration

A radiographic examination suggested that no obvious new bony tissues were formed in the GF group, although all the defects in GF-rhBMP2 group were completely repaired. The radiopacity in GF-DFO scaffolds was significantly higher than that in the GF group but lower than that in the GF-rhBMP2 group (lower panel, Figure 7). The macroviews of the histologic slides were included to show the positions of the scaffolds, bone defects, and the adjacent tissues (upper panel, Figure 7). Higher magnification histological observation confirmed that very few new bone (pink color) was formed inside the transplanted scaffolds (purple color) in GF groups. New bone can be easily differentiated from residual bone by the location and structure of the new bone. The bone located inside of the transplanted scaffolds was newly formed bone and is more interesting to our studies. Only one sample (1/5) had a small amount of new bone observed in the scaffold out of the five total transplants. However, all the samples from GF-rhBMP2 group (7/7) had potent new bone/marrow formed throughout the scaffolds and completely bridged the critical defects (Figure 8). Consistent with the observations from radiographic examination, H&E staining indicated that majority of the samples from GF-DFO group (6/8) formed significant new bone inside the scaffolds (Figure 8), although variations of new bone area in GF-DFO group were noticed. The average new bone area was much lower in the GF-DFO produced endogenous bone formation compared to that in the exogenous rhBMP2 (1.5 μg/scaffold) induced bone formation (3.87 vs 22.08%, Table 2). Moreover, distinct structures of the newly formed bone were noticed between exogenous rhBMP2 and GF-DFO groups. For example, mature marrow tissues, including hematopoietic cells and fat cells, were present in the bone formed by the exogenous rhBMP2 group, but very few marrow tissues were found in the bone generated by the GF-DFO group. Therefore, these in vivo data indicated that DFO-immobilized GF scaffolds were able to significantly promote endogenous bone formation in the mouse critical cranial bone defect model.

4. DISCUSSION

Local release of DFO from a material is emerging as an alternative strategy to reduce the potential off-target effects derived from conventional injections.[8,20,33] However, the

significant cytotoxicity even at concentration as low as 5 μM[34] with the free native DFO molecules cannot be mitigated by applying just physical interaction-based techniques (i.e., absorption). To address this challenge, we did this proof-of-concept study by covalently immobilizing DFO onto a GF scaffold (GF-DFO) through amide linkages. GF-DFO scaffolds showed no cytotoxicity on hMSCs; however, relatively low cytotoxicity on HUVECs was shown at a high dosage of DFO. On the basis of the cell response change and elevated VEGF level, we can conclude that the cytotoxicity of DFO was significantly reduced after covalent conjugation, while functionality was maintained. The mechanism for the decreased DFO cytotoxicity is still elusive although it was thought, at least partially, to be due to the inability of DFO to permeate cell membrane after conjugation to polymers.[21]

HUVECs and hMSCs were used in our study because they are the most widely studied cell models for angiogenesis and osteogenesis, where both are important for bone formation. The mild VEGF producing ability of HUVECs was possibly due to the inappropriate oxygen level according to a recent report on DFO.[20] Interactions between HUVECs and hMSCs greatly contribute to both angiogenesis and osteogenesis from both in vitro and in vivo studies.[35–38] Therefore, our data from two cell types will provide more related information on cell response studies of DFO-decorated scaffold for bone regeneration compared to data using just one cell type.

In addition to the in vitro activities, our in vivo data strongly suggested that DFO-decorated biomimicking GF scaffolds were able to significantly promote endogenous bone formation without any exogenous cells or growth factors transplanted. It is not surprising to see the reported benefits of employing DFO for bone formation because we know DFO is a potent hypoxia-mimetic agent that activates hypoxia mediated angiogenesis.[5,19,21,22,39] The elevated VEGF expression in both hMSCs and HUVECs from in vitro data also suggested GF-DFO scaffolds promoted osteogenesis likely through angiogenesis, although we did not find significantly improved new blood vessels in transplanted scaffolds from the one-week histological samples (data not shown). More time points at the early stage after surgery may be needed to show the angiogenesis change in our future work. One recent publication proved that scaffold-based local release of DFO was a valid strategy to improve bone formation through improving angiogenesis, although they used different release method (i.e., physical absorption), scaffold (poly(lactic-*co*-glycolic acid), PLGA), and animal model (long bone defect).[31] In addition to angiogenesis, immobilized DFO may promote osteogenesis through other angiogenesis-independent ways because multiple targets were reported once HIFs signaling pathway was activated.[40,41] Furthermore, many studies reported that hypoxic conditions are able to directly modulate MSC proliferation and differentiation to osteoblasts, though controversial results were noted, which have been summarized in a recent review article.[41] We did not find that DFO could directly increase hMSCs osteogenic differentiation in vitro (data not shown). Further studies are needed to understand the potential mechanisms by which DFO/HIF-1's direct effects on MSCs functions for osteogenic differentiation. Our data indicated that DFO significantly increased BMP2 expression in HUVECs but not in hMSCs. Moreover, the base level of BMP2 in HUVECs was much higher than that in hMSCs based on our ELISA data. These interesting results indicated that DFO might indirectly increase mesenchymal cells osteogenic differentiation by way of targeting endothelial cells. One recent in vivo study also suggested

that vascular tissues were a primary source of BMP2 expression during bone formation in a mouse model.[42] Considering both VEGF and BMP2 expression pattern and function in HUVECs and hMSCs, we reasoned that DFO could coordinately promote osteogenesis and angiogenesis via a mutually supporting set of paracrine loops. Our previous work demonstrated that a 3D porous, biodegradable nanofibrous scaffold was advantageous over current approaches in tissue regeneration.[43–46] Additional osteogenic signals (e.g., BMPs/osteoprogenitors), however, were still required, and must be supplemented with nanofibrous scaffold for bone regeneration. DFO functionalized GF scaffolds (GF-DFO) are able to promote significant bone formation potentially by improving endogenous reparative cells and signals. The efficacy of DFO to promote bone formation still needs to be further improved because the critical bone defects cannot be completely repaired by GF-DFO scaffolds in six weeks. In spite of this, hypoxia-mimetic nanofibrous scaffolds are intriguing for potential clinical applications without using any exogenous biological agents (e.g., cells and growth factors).

5. CONCLUSIONS

In this study, the iron chelator and hypoxia-mimetic agent DFO was covalently conjugated to biomimetic gelatin nanofibrous scaffolds. The iron binding ability of DFO was retained after cross-linking with gelatin without affecting the micro/macrostructure of the scaffold. In vitro results showed that the cytotoxicity of GF-DFO nanofibrous scaffolds on both HUVEC and hMSC was significantly decreased compared to that of neat DFO, and GF-DFO nanofibrous scaffolds still can significantly increase VEGF expression in these cells. It is interesting to note that hMSC exhibited a higher VEGF expression, while HUVEC had a higher BMP2 expression response to the same dosage of DFO. Our in vivo data indicated that GF-DFO scaffolds significantly improved bone formation after six weeks in a critical-sized cranial bone defect mouse model. These encouraging data suggested that it is a promising strategy to promote endogenous bone formation using a hypoxia-mimicking nanofibrous scaffold.

Supplementary Material

Refer to Web version on PubMed Central for supplementary material.

Acknowledgments

This work was supported by National Science Foundation/EPSCoR (Award IIA-1335423) and by the South Dakota Board of Regents Competitive Research Grant (CRG) (Award UP1500172). The authors thank the assistance provided by Sanford Research Imaging Core and Molecular Pathology Core, which is supported by the National Institutes of Health COBRE grants (P20 GM103620 and P20 GM103548). The authors thank Drs. Xiaohua Liu and Erin B. Harmon for their outstanding technical assistance. The authors also thank Dr. Daniel Engebretson for his assistance in reading and editing the manuscript.

References

1. Gothard D, Smith E, Kanczler J, Rashidi H, Qutachi O, Henstock J, Rotherham M, El Haj A, Shakesheff KM, Oreffo RO. Tissue Engineered Bone Using Select Growth Factors: A Comprehensive Review of Animal Studies and Clinical Translation Studies in Man. Eur Cell Mater. 2014; 28:166–208. [PubMed: 25284140]

2. Haidar ZS, Hamdy RC, Tabrizian M. Delivery of Recombinant Bone Morphogenetic Proteins for Bone Regeneration and Repair. Part A: Current Challenges in BMP Delivery. Biotechnol Lett. 2009; 31:1817–1824. [PubMed: 19690804]

3. Zakrzewski JL, Van Den Brink MR, Hubbell JA. Overcoming Immunological Barriers in Regenerative Medicine. Nat Biotechnol. 2014; 32:786–794. [PubMed: 25093888]

4. Ankrum JA, Ong JF, Karp JM. Mesenchymal Stem Cells: Immune Evasive, Not Immune Privileged. Nat Biotechnol. 2014; 32:252–260. [PubMed: 24561556]

5. Wang Y, Wan C, Deng L, Liu X, Cao X, Gilbert SR, Bouxsein ML, Faugere MC, Guldberg RE, Gerstenfeld LC, Haase VH, Johnson RS, Schipani E, Clemens TL. The Hypoxia–inducible Factor α Pathway Couples Angiogenesis to Osteogenesis During Skeletal Development. J Clin Invest. 2007; 117:1616–1626. [PubMed: 17549257]

6. Wan C, Gilbert SR, Wang Y, Cao X, Shen X, Ramaswamy G, Jacobsen KA, Alaql ZS, Eberhardt AW, Gerstenfeld LC, Einhorn TA, Deng L, Clemens TL. Activation of the Hypoxia-inducible Factor–1α Pathway Accelerates Bone Regeneration. Proc Natl Acad Sci U S A. 2008; 105:686–691. [PubMed: 18184809]

7. Zou D, Zhang Z, He J, Zhang K, Ye D, Han W, Zhou J, Wang Y, Li Q, Liu X, Zhang X, Wang S, Hu J, Zhu C, Zhang W, Zhou Y, Fu H, Huang Y, Jiang X. Blood Vessel Formation in the Tissue–engineered Bone with the Constitutively Active Form of HIF–1α Mediated BMSCs. Biomaterials. 2012; 33:2097–2108. [PubMed: 22172336]

8. Hertzberg BP, Holt JB, Graff RD, Gilbert SR, Dahners LE. An Evaluation of Carrier Agents for Desferoxamine, An Up–regulator of Vascular Endothelial Growth Factor. J Biomater Appl. 2013; 27:1046–1054. [PubMed: 22262572]

9. Hou Z, Nie C, Si Z, Ma Y. Deferoxamine Enhances Neovascularization and Accelerates Wound Healing in Diabetic Rats via the Accumulation of Hypoxia–inducible Factor1α. Diabetes Res Clin Pract. 2013; 101:62–71. [PubMed: 23726275]

10. Bao P, Kodra A, Tomic-Canic M, Golinko MS, Ehrlich HP, Brem H. The Role of Vascular Endothelial Growth Factor in Wound Healing. J Surg Res. 2009; 153:347–358. [PubMed: 19027922]

11. Dai J, Rabie ABM. VEGF: An Essential Mediator of Both Angiogenesis and Endochondral Ossification. J Dent Res. 2007; 86:937–950. [PubMed: 17890669]

12. Maes C, Carmeliet G, Schipani E. Hypoxia-driven Pathways in Bone Development, Regeneration and Disease. Nat Rev Rheumatol. 2012; 8:358–366. [PubMed: 22450551]

13. Forsythe JA, Jiang BH, Iyer NV, Agani F, Leung SW, Koos RD, Semenza GL. Activation of Vascular Endothelial Growth Factor Gene Transcription by Hypoxia-inducible Factor 1. Mol Cell Biol. 1996; 16:4604–4613. [PubMed: 8756616]

14. Ceradini DJ, Gurtner GC. Homing to Hypoxia: HIF–1 as A Mediator of Progenitor Cell Recruitment to Injured Tissue. Trends Cardiovasc Med. 2005; 15:57–63. [PubMed: 15885571]

15. Ceradini DJ, Kulkarni AR, Callaghan MJ, Tepper OM, Bastidas N, Kleinman ME, Capla JM, Galiano RD, Levine JP, Gurtner GC. Progenitor Cell Trafficking is Regulated by Hypoxic Gradients Through HIF–1 Induction of SDF–1. Nat Med. 2004; 10:858–864. [PubMed: 15235597]

16. Brittenham GM. Iron–chelating Therapy for Transfusional Iron Overload. N Engl J Med. 2011; 364:146–156. [PubMed: 21226580]

17. Olivieri NF, Brittenham GM. Iron–chelating Therapy and the Treatment of Thalassemia. Blood. 1997; 89:739–761. [PubMed: 9028304]

18. Bernhardt PV. Coordination Chemistry and Biology of Chelators for the Treatment of Iron Overload Disorders. Dalton Trans. 2007; 14:3214–3220.

19. Shen X, Wan C, Ramaswamy G, Mavalli M, Wang Y, Duvall CL, Deng LF, Guldberg RE, Eberhart A, Clemens TL, Gilbert SR. Prolyl Hydroxylase Inhibitors Increase Neoangiogenesis and Callus Formation Following Femur Fracture in Mice. J Orthop Res. 2009; 27:1298–1305. [PubMed: 19338032]

20. Saito T, Tabata Y. Hypoxia–induced Angiogenesis is Increased by the Controlled Release of Deferoxiamine from Gelatin Hydrogels. Acta Biomater. 2014; 10:3641–3649. [PubMed: 24769115]

21. Farberg AS, Jing XL, Monson LA, Donneys A, Tchanque-Fossuo CN, Deshpande SS, Buchman SR. Deferoxamine Reverses Radiation Induced Hypovascularity During Bone Regeneration and Repair in the Murine Mandible. Bone. 2012; 50:1184–1187. [PubMed: 22314387]
22. Guzey S, Ozturk S, Aykan A, Avsever H, Karslioglu Y, Ertan A. The Effects of Desferroxamine on Bone and Bone Graft Healing in Critical-Size Bone Defects. Ann Plast Surg. 2014; 134:62–63.
23. Hamilton JL, Kizhakkedathu JN. Polymeric Nanocarriers for the Treatment of Systemic Iron Overload. Mol Cell Ther. 2015; 3:3. [PubMed: 26056604]
24. Hallaway PE, Eaton JW, Panter SS, Hedlund BE. Modulation of Deferoxamine Toxicity and Clearance by Covalent Attachment to Biocompatible Polymers. Proc Natl Acad Sci U S A. 1989; 86:10108–10112. [PubMed: 2481311]
25. Imran ul-haq M, Hamilton JL, Lai BF, Shenoi RA, Horte S, Constantinescu I, Leitch HA, Kizhakkedathu JN. Design of Long Circulating Nontoxic Dendritic Polymers for the Removal of Iron In Vivo. ACS Nano. 2013; 7:10704–10716. [PubMed: 24256569]
26. Rossi NA, Mustafa I, Jackson JK, Burt HM, Horte SA, Scott MD, Kizhakkedathu JN. In Vitro Chelating, Cytotoxicity, and Blood Compatibility of Degradable Poly (ethylene glycol)-based Macromolecular Iron Chelators. Biomaterials. 2009; 30:638–648. [PubMed: 18977029]
27. Sun Y, Jiang Y, Liu Q, Gao T, Feng JQ, Dechow P, D'Souza RN, Qin C, Liu X. Biomimetic Engineering of Nanofibrous Gelatin Scaffolds with Noncollagenous Proteins for Enhanced Bone Regeneration. Tissue Eng, Part A. 2013; 19:1754–1763. [PubMed: 23469769]
28. Lei B, Shin K–H, Noh D–Y, Jo I–H, Koh Y–H, Choi W–Y, Ki HE. Nanofibrous Gelatin–silica Hybrid Scaffolds Mimicking the Native Extracellular matrix (ECM) Using Thermally Induced Phase Separation. J Mater Chem. 2012; 22:14133–14140.
29. Qu T, Liu X. Nano–structured Gelatin/Bioactive Glass Hybrid Scaffolds for the Enhancement of Odontogenic Differentiation of Human Dental Pulp Stem Cells. J Mater Chem B. 2013; 1:4764–4772.
30. Liu X, Ma PX. Phase Separation, Pore Structure, and Properties of Nanofibrous Gelatin Scaffolds. Biomaterials. 2009; 30:4094–4103. [PubMed: 19481080]
31. Jia P, Chen H, Kang H, Qi J, Zhao P, Jiang M, Guo L, Zhou Q, Qian ND, Zhou HB, Xu YJ, Fan Y, Deng LF. Deferoxamine Released from Poly(lactic-co-glycolic acid) Promotes Healing of Osteoporotic Bone Defect via Enhanced Angiogenesis and Osteogenesis. J Biomed Mater Res, Part A. 2016; 104:2515–2527.
32. Sun H, Jung Y, Shiozawa Y, Taichman RS, Krebsbach PH. Erythropoietin Modulates the Structure of Bone Morphogenetic Protein 2–Engineered Cranial Bone. Tissue Eng, Part A. 2012; 18:2095–2105. [PubMed: 22703029]
33. Chen H, Jia P, Kang H, Zhang H, Liu Y, Yang P, Yan Y, Zuo G, Guo L, Jiang M, Qi J, Liu Y, Cui W, Santos HA, Deng L. Upregulating Hif–1α by Hydrogel Nanofibrous Scaffolds for Rapidly Recruiting Angiogenesis Relative Cells in Diabetic Wound. Adv Healthcare Mater. 2016; 5:907–918.
34. Poot M, Rabinovitch PS, Hoehn H. Free Radical Mediated Cytotoxicity of Desferrioxamine. Free Radical Res Commun. 1989; 6:323–328. [PubMed: 2477312]
35. Saleh FA, Whyte M, Ashton P, Genever PG. Regulation of Mesenchymal Stem Cell Activity by Endothelial Cells. Stem Cells Dev. 2011; 20:391–403. [PubMed: 20536359]
36. Koob S, Torio-Padron N, Stark GB, Hannig C, Stankovic Z, Finkenzeller G. Bone Formation and Neovascularization Mediated by Mesenchymal Stem Cells and Endothelial Cells in Critical-sized Calvarial Defects. Tissue Eng, Part A. 2011; 17:311–321. [PubMed: 20799886]
37. Saleh F, Whyte M, Genever P. Effects of Endothelial Cells on Human Mesenchymal Stem Cell Activity in A Three–dimensional In Vitro Model. Eur Cell Mater. 2011; 22:e57.
38. Kang Y, Kim S, Bishop J, Khademhosseini A, Yang Y. The Osteogenic Differentiation of Human Bone Marrow MSCs on HUVEC-derived ECM and β–TCP Scaffold. Biomaterials. 2012; 33:6998–7007. [PubMed: 22795852]
39. Donneys A, Weiss DM, Deshpande SS, Ahsan S, Tchanque-Fossuo CN, Sarhaddi D, Levi B, Goldstein SA, Buchman SR. Localized Deferoxamine Injection Augments Vascularity and Improves Bony Union in Pathologic Fracture Healing after Radiotherapy. Bone. 2013; 52:318–325. [PubMed: 23085084]

40. Stiers P–J, van Gastel N, Carmeliet G. Targeting the Hypoxic Response in Bone Tissue Engineering: A Balance Between Supply and Consumption to Improve Bone Regeneration. Mol Cell Endocrinol. 2016; 432:96–105. [PubMed: 26768117]

41. Drager J, Harvey EJ, Barralet J. Hypoxia Signalling Manipulation for Bone Regeneration. Expert Rev Mol Med. 2015; 17:e6. [PubMed: 25900271]

42. Matsubara H, Hogan DE, Morgan EF, Mortlock DP, Einhorn TA, Gerstenfeld LC. Vascular Tissues are A Primary Source of BMP2 Expression during Bone Formation Induced by Distraction Osteogenesis. Bone. 2012; 51:168–180. [PubMed: 22391215]

43. Hu J, Smith LA, Feng K, Liu X, Sun H, Ma PX. Response of Human Embryonic Stem Cell–Derived Mesenchymal Stem Cells to Osteogenic Factors and Architectures of Materials During In Vitro Osteogenesis. Tissue Eng, Part A. 2010; 16:3507–3514. [PubMed: 20594153]

44. Feng K, Sun H, Bradley MA, Dupler EJ, Giannobile WV, Ma PX. Novel Antibacterial Nanofibrous PLLA Scaffolds. J Controlled Release. 2010; 146:363–369.

45. Sun H, Feng K, Hu J, Soker S, Atala A, Ma PX. Osteogenic Differentiation of Human Amniotic Fluid–derived Stem Cells Induced by Bone Morphogenetic Protein–7 and Enhanced by Nanofibrous Scaffolds. Biomaterials. 2010; 31:1133–1139. [PubMed: 19857889]

46. Xu T, Miszuk JM, Zhao Y, Sun H, Fong H. Electrospun Polycaprolactone 3D Nanofibrous Scaffold with Interconnected and Hierarchically Structured Pores for Bone Tissue Engineering. Adv Healthcare Mater. 2015; 4:2238–2246.

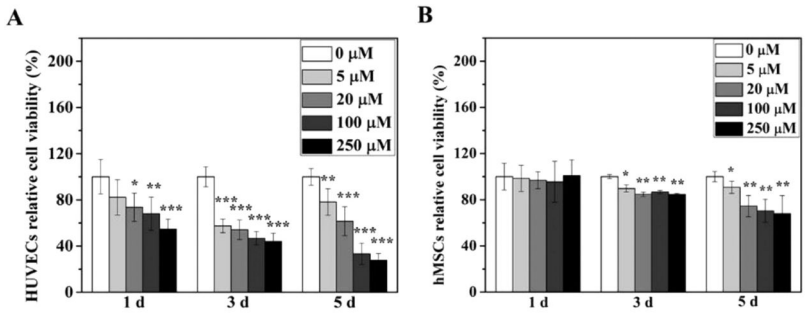

Figure 1.

Cytotoxicity of DFO on HUVECs and hMSCs. Cell viability of HUVECs (A) and hMSCs (B) was studied after the cells were cultured in medium supplemented with different concentration of DFO for 1, 3, and 5 days ($n = 6$). Data are expressed as mean ± SD (*$p < 0.05$; **$p < 0.01$; ***$p < 0.001$).

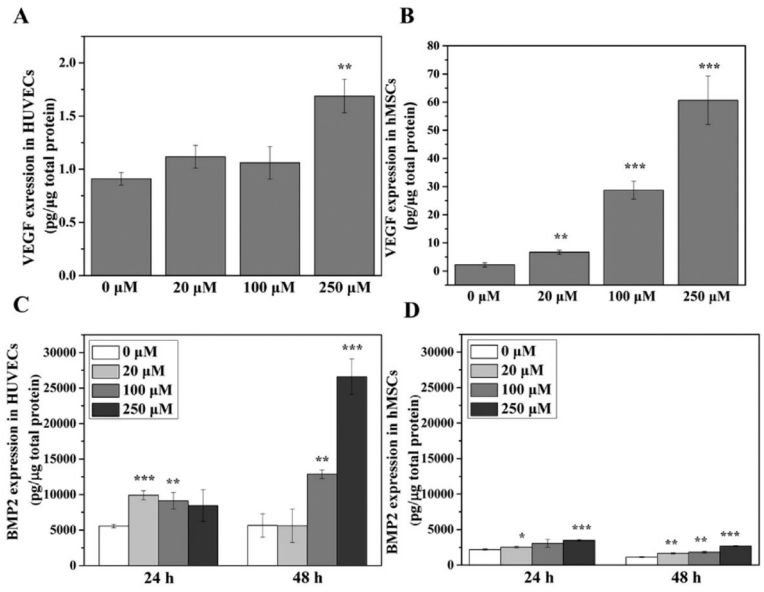

Figure 2.

DFO-induced VEGF and BMP2 expression in HUVECs and hMSCs. VEGF expression in HUVECs (A) and hMSCs (B) was measured after the cells were cultured in medium supplemented with different concentrations of DFO for 24 h ($n = 3$). BMP2 expression in HUVECs (C) and hMSCs (D) was measured after the cells were cultured in medium supplemented with different concentrations of DFO for 24 and 48 h ($n = 3$). Data are expressed as mean ± SD (*$p < 0.05$; **$p < 0.01$; ***$p < 0.001$).

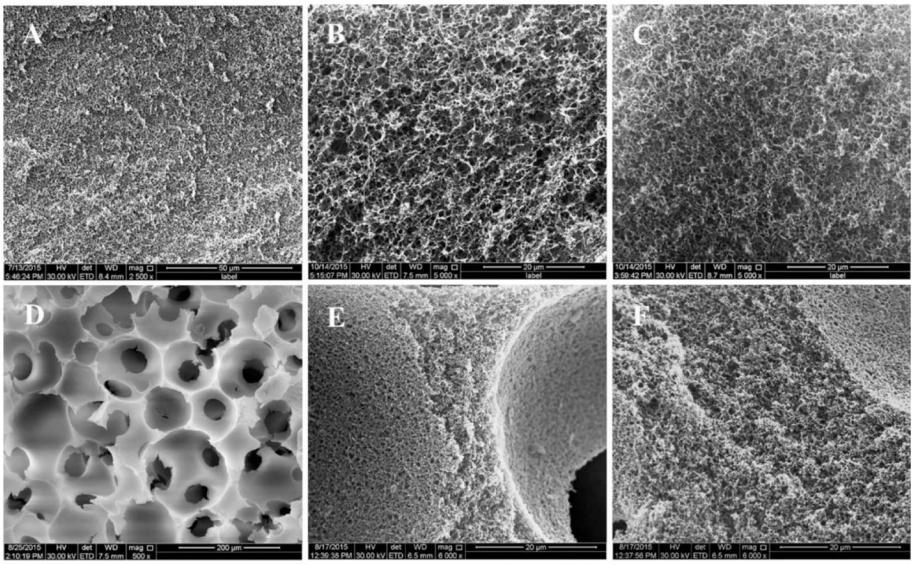

Figure 3.

SEM images of gelatin scaffolds. Both 2D and 3D GF scaffold morphology was observed by SEM after DFO conjugation. 2D GF at low magnification (A, scale bar = 50 μm) and high magnification (B, scale bar = 20 μm). 2D GF-DFO at high magnification (C, scale bar = 20 μm). 3D GF at low magnification (D, scale bar = 200 μm) and high magnification (E, scale bar = 20 μm). 3D GF-DFO scaffolds at high magnification (F, scale bar = 20 μm).

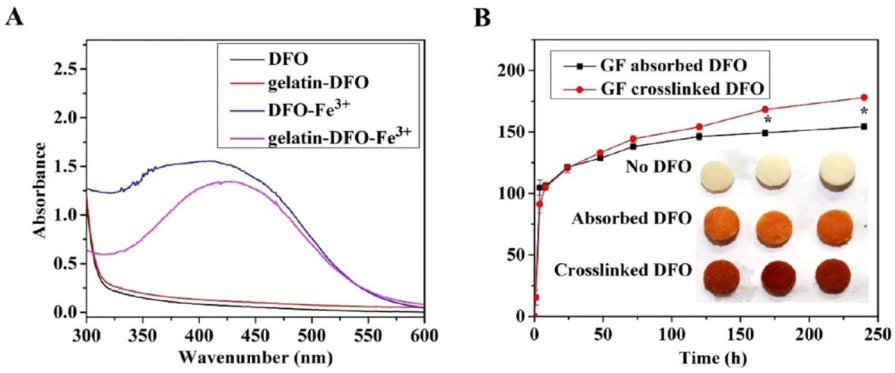

Figure 4.

Iron binding test and in vitro DFO release. UV–vis spectra of aqueous solute irons of DFO, gelatin-DFO, DFO-Fe^{3+}, and gelatin-DFO-Fe^{3+} (A). DFO released from absorbed (black) or cross-linked (red) GF-DFO scaffolds (B) were measured by UV–vis spectra. The retained DFO in the GF scaffolds after 10 days of release were visualized by captured Fe^{3+} (inset of B).

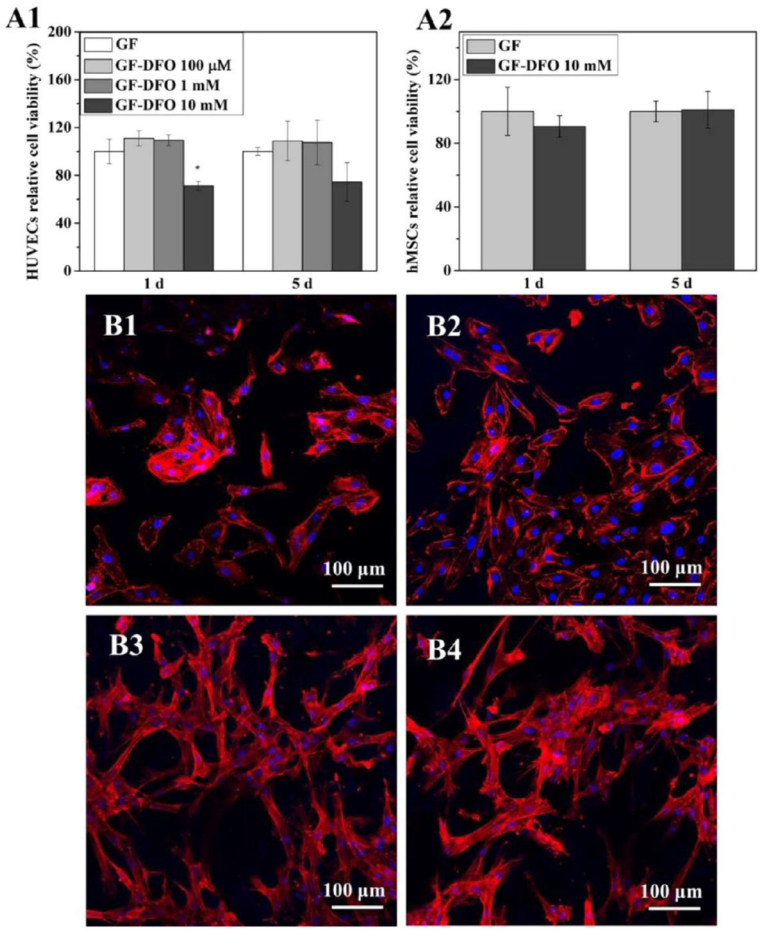

Figure 5.

Cell viability and morphology on DFO conjugated-scaffolds. Cell viability of HUVECs (A1) and hMSCs (A2) were studied after the cells were cultured on GF and GF-DFO scaffolds for 1 and 5 days ($n = 3$). Confocal images were taken of HUVECs grown on GF (B1) and GF-DFO (B2) scaffolds after 16 h and of hMSCs grown on GF (B3) and GF-DFO (B4) scaffolds after 16 h. Actin cytoskeletons are shown in red, while cell nuclei are shown in blue. Scale bar =100 μm. Data are expressed as mean ± SD (*$p < 0.05$).

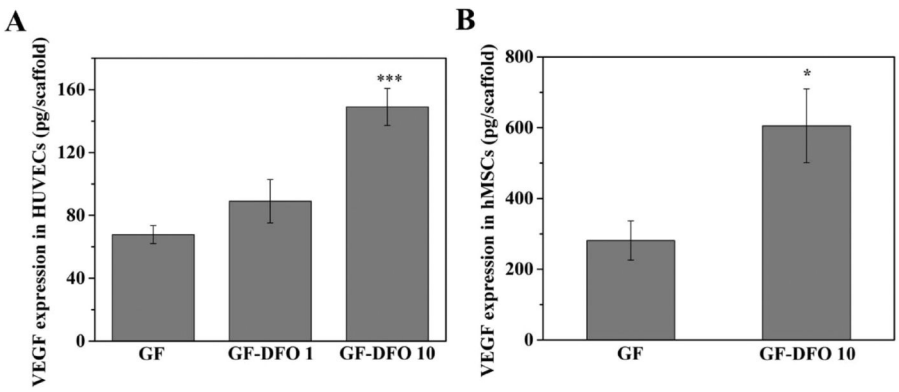

Figure 6.

VEGF expression in HUVECs and hMSCs cultured on DFO conjugated-scaffolds. VEGF expression in HUVECs (A) and hMSCs (B) was measured after the cells were cultured on GF and GF-DFO scaffolds for 24 h ($n = 3$). Data are expressed as mean ± SD (*$p < 0.05$; ***$p < 0.001$).

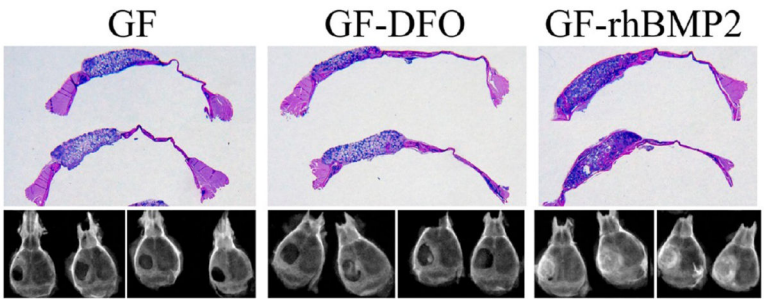

Figure 7.

Radiographic examination and macroview of the histological samples. GF, GF-DFO, and GF-rhBMP2 groups after six weeks of implantation. Representative data are shown (n = 5–8).

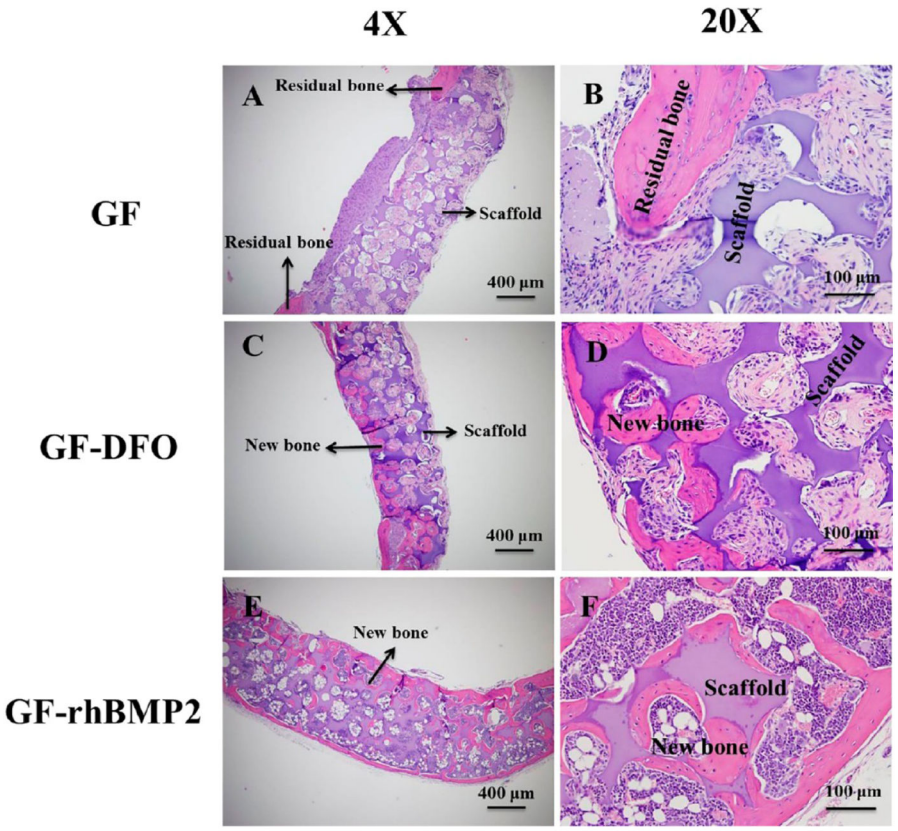

Figure 8.

Histologic examination. H&E staining of repaired calvarias in the (A and B) GF group, (C and D) GF-DFO group, and (E and F) GF-rhBMP2 group after six weeks of implantation in vivo. Scar bar = 400 μm in A, C, and E. Scar bar = 100 μm in B, D, and F. Representative data are shown (n = 5–8).

Table 1

Structural Parameters of 2D and 3D GF Scaffolds

GF scaffold type	gelatin concentration (%)	fiber diameter (nm)	fiber length (nm)	porosity (%)
2D	5	180 ± 54	1070 ± 232	89.17 ± 0.13
3D	7.5	130 ± 42	716 ± 175	95.90 ± 0.64

Table 2

New Bone Formation in GF, GF-DFO, and GF-rhBMP2 Groups after Six Weeks of Implantation

	GF	GF-DFO	GF-rhBMP2
scaffolds with new bone formation/total scaffolds	1/5	6/8	7/7
new bone area fraction	0.20%	3.87%	22.08%